Available online at www.sciencedirect.com
ScienceDirect
Trans. Nonferrous Met. Soc. China 25(2015) 3855−3864
Transactions of Nonferrous Metals Society of China
www.tnmsc.cn

Hot deformation behavior and microstructure evolution of 1460 Al−Li alloy

Sheng XIANG[1], Dan-yang LIU[1], Rui-hua ZHU[1], Jin-feng LI[1], Yong-lai CHEN[2], Xu-hu ZHANG[2]

1. School of Materials Science and Engineering, Central South University, Changsha 410083, China;
2. Aerospace Research Institute of Materials and Processing Technology, Beijing 100076, China

Received 12 January 2015; accepted 22 April 2015

Abstract: The hot deformation behavior and microstructure evolution of 1460 Al−Li alloy were investigated by isothermal compression test conducted at various strain rates (10^{-3}−10 s^{-1}) and temperatures (573−773 K). The flow stress curves were corrected by considering the friction at the platen/specimen interface and the temperature change due to the deformation heating. The effects of strain, strain rate and temperature on the deformation behavior were characterized by the Zener−Hollomon parameter in a hyperbolic-sine equation, and the constitutive equations were established according to the peak flow stress associated with dynamic recovery, dynamic recrystallization and the dissolution of T_1 phases. In the entire strain rate and temperature range, the prediction capabilities of the developed constitutive equation are proved to be feasible and effective with a linear correlation coefficient and an average absolute relative error coefficient of 0.9909 and 6.72%, respectively.

Key words: 1460 Al−Li alloy; friction correction; temperature rise correction; constitutive equation; hot deformation behavior

1 Introduction

Al alloys containing a certain amount of Li are recognized as the most promising aeronautical materials, which offer significant improvements in aero-structural performance through density reduction, strength increase and low temperature resistance, etc [1−3]. Among these Al−Li alloys, 1460 Al−Li alloy was developed in Russia and successfully applied in Energia rocket tank. However, its deformation under as-cast condition at elevated temperature is difficult, not merely because of its low ductility but also due to its high sensitivity to hot cracking and dynamic instability. Therefore, it is important to understand its hot deformation behavior so as to design a suitable process schedule.

Although hot deformation behavior of various Al alloys have been reported in Refs. [4−6], the thermo-mechanical processing parameters associated with 1460 Al−Li alloy have not yet been identified or optimized. Among these parameters, the flow stress and the Zener−Hollomon parameter play a fundamental role to construct its constitutive equation during the deformation process. So far, numerous articles concerning the constitutive relations have been reported. LAASRAOUI and JONAS [7] put forward a model to determine the flow stress of steel, which was an evolution equation considering dislocation density and fractional softening by dynamic recrystallization. LIN and LIU [8] proposed a new material parameter (L) sensitive to the deformation heating and strain rate for developing the constitutive equation. LANGKRUIS et al [9] assessed five constitutive models with varying numbers of fitting parameters for modeling the stress−strain curves of four high-purity Al−Mg−Si alloys, and concluded that the general exponential saturation equation combining with the hyperbolic sine law was the most promising model.

Nevertheless, the friction at the platen/specimen interface and the temperature rise due to the deformation heating during the deformation process will inevitably cause the data distortion. These two factors should be taken into account when the constitutive equation is established. Hence, EBRAHIMI and NAJAFIZADEH [10] used barreling degree during the barrel compression test to calculate the constant friction factor (m). Only the physical measurement of shape change was involved in this method, which evidently simplified the evaluation of the interfacial frictional conditions and thus easily corrected the experimental stress. As for the friction

Foundation item: Project supported by the Nonferrous Metal Oriented Advanced Structural Materials and Manufacturing Cooperative Innovation Center; Project (2013JSJJ0001) supported by the Teachers' Research Foundation of Central South University, China
Corresponding author: Jin-feng LI; Tel: +86-731-8830270; E-mail: lijinfeng@csu.edu.cn
DOI: 10.1016/S1003-6326(15)64033-X

correction, various mechanical properties of the material and the forming loads are often taken into consideration in some models [11−13]. In the case of the temperature correction, a adiabatic correction factor (η) was applied by GOETZ and SEMIATIN [14] to calculate the temperature change resulted from the deformation heating during the uniaxial compression test, which demonstrated that η was not constant with strain, but decreased with increasing the strain from an initial value of 1.0. It was noted that most studies concerning the flow stress during the hot deformation process only considered the friction correction [11−13] and temperature rise correction [15,16].

In this study, the deformation heating together with the constant friction factor was considered to correct the flow stress curves of 1460 Al−Li alloy during the uniaxial compression process. The corrected stress was then applied to establishing appropriate constitutive equations. Meanwhile, the microstructural variation during the deformation process was observed.

2 Experimental

The as-cast 1460 Al−Li alloy was used in the hot compression test. Its chemical composition is presented in Table 1. After homogenization at 803 K for 24 h, the cylindrical specimens with dimensions of 12 mm in height and 8 mm in diameter were machined out from the ingot.

Table 1 Chemical composition of 1460 Al−Li alloy (mass fraction, %)

Li	Cu	Sc	Zr	Ce	Ti	Al
2.13	3.0	0.12	0.12	0.015	0.05	Bal.

The hot compression tests were carried out with a thermo-mechanical simulator Gleeble Systems 3180 at ambient pressure. For temperature control during the tests, thermocouples were welded onto the middle of surfaces of the specimens. Between the specimen and the tungsten carbide, a punched graphite slice (thickness of 0.12 mm) with a thin film of nickel-containing paste was placed to reduce the friction. Before compression, the specimens were resistance-heated at a rate of 5 K/s and then kept at the preset temperature for 120 s. The test temperature ranged from 573 to 773 K with a step of 50 K and the strain rates ($\dot{\varepsilon}$) were 0.001, 0.01, 0.1, 1 and 10 s^{-1}, respectively. After deformation at a final strain (ε) of 0.5, the specimen was immediately water-quenched to ambient temperature. Finally, the microstructures of the deformed specimens were observed by an FEI Tecnai G^2 20 transmission electron microscope (TEM).

3 Results and discussion

3.1 Flow stress correction

During the compression process, there exist friction at the platen/specimen interface and temperature changes due to the deformation heating. The correction of the initial experimental flow stress must be conducted to accurately predict the hot deformation behavior of the alloy.

In the compression test for 1460 Al−Li alloy, the clear bulges can be seen in the middle of the final specimen (Fig. 1), though the lubricant (graphite slice) is used to minimize the interfacial friction. With higher temperature and larger deformation degree, the interface area between the specimen and dies increases. The interfacial friction becomes more and more evident as the compression proceeds, and the deformation is increasingly heterogeneous. Therefore, the consideration of interfacial friction effects should be significant in the flow stress correction. Some shape parameters of the specimens must be measured before and after deformation. According to the friction correction model proposed by EBRAHIMI and NAJAFIZADEH [10], the experimental flow stress can be corrected by the following equation:

$$\frac{P_{\text{ave}}}{\sigma_0}=8b\frac{R}{H}\left[\left(\frac{1}{12}+\frac{H^2}{R^2b^2}\right)^{3/2}-\frac{H^3}{R^3b^3}-\frac{m}{24\sqrt{3}}\frac{\mathrm{e}^{-b/2}}{\mathrm{e}^{-b/2}-1}\right] \tag{1}$$

where P_{ave} is the external nominal stress imposed on the cylinder specimen, σ_0 is the stress after the friction correction, R is the nominal radius of cylinder after deformation, which equals $R_0\sqrt{H_0/h}$, H_0 and h denote the heights of the undeformed and deformed specimens, respectively, and H is the height of cylinder after deformation. The parameters of m and b represent the constant friction coefficient and the barrel parameter, respectively, which can be evaluated as follows [10]:

$$m=\frac{(R/H)b}{(4/\sqrt{3})-(2b/3\sqrt{3})} \tag{2}$$

$$b=4\frac{\Delta R}{R}\frac{H}{\Delta H} \tag{3}$$

where

$\Delta R=R_{\text{M}}-R_{\text{T}}$,

$R_{\text{T}}=\sqrt{3\frac{H_0}{h}R_0^2-2R_{\text{M}}^2}$,

$\Delta H=H_0-h$.

R_{M} and R_{T} are the maximum and top radius of the deformed specimens, respectively. R_0 stands for the initial radius of the specimens.

During the compression process, there exists deformation heating. At high strain rates, there is no time for heat to dissipate and the specimen temperature rises to a variable extent. Even at slow deformation rates, the deformation energy will not completely escape through the anvils or to the ambient air. Furthermore, only about 3%−5% of the deformation energy stays in the material as stored energy, but the rest deformation energy is fully capable of raising the temperature of test specimens [17]. Its real temperature is therefore higher than the set temperature, and the flow stress should be corrected by considering the temperature rise caused by the deformation heating.

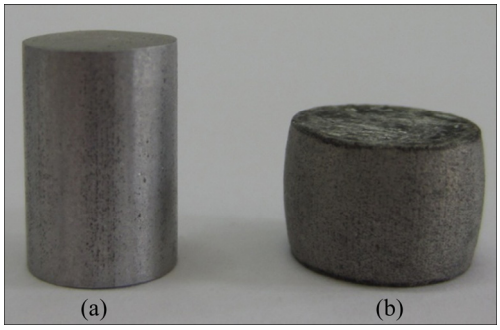

Fig. 1 Cylinders before (a) and after (b) hot compression test

According to the methods proposed by GOETZ and SEMIATIN [14], the additional temperature rise (ΔT) due to the deformation heating is expressed by the following equation:

$$\Delta T = \frac{0.95\eta \int_{\varepsilon_0}^{\varepsilon_0+\Delta\varepsilon} \sigma d\varepsilon}{\rho C_{\mathrm{p}}} \tag{4}$$

where ρ and C_{p} are the material constants, representing the density and the specific heat capacity of 1460 Al−Li alloy, respectively. η is the adiabatic correction factor calculated by the following equations [14]:

$$\eta = \left(1 + \frac{h\Delta\varepsilon}{\dot{\varepsilon} X_{\mathrm{W}} \rho C_{\mathrm{p}}}\right)^{-1} \tag{5}$$

$$p = \left(\frac{X_{\mathrm{W}}}{K_{\mathrm{W}}} + \frac{1}{q} + \frac{X_{\mathrm{D}}}{K_{\mathrm{D}}}\right)^{-1} \tag{6}$$

where X_{W} is one-half the workpiece height, K_{W} is the workpiece thermal conductivity, q is the interface heat-transfer coefficient of the flake graphite, X_{D} is the distance from the die surface to the die interior where the temperature is constant, and K_{D} is the die thermal conductivity. The parameter p in Eq. 6 is considered as an overall heat-transfer coefficient.

Based on the above theories concerning friction correction and temperature rise correction, the flow stress during the whole compression process can be modified. Figure 2 shows the measured original stress−strain curves and corrected stress−strain curves (considering the effects of friction and temperature rise) of the 1460 Al−Li alloy under various conditions. The corrected curves are obviously different from the original ones. Compared with the original ones, the flow stress after friction correction only decreases. Meanwhile, their relative difference becomes larger as the strain increases, indicating greater influence of friction at higher strain.

After the temperature rise correction and the friction correction, the corrected flow stress increases, because the additional temperature rise caused by deformation heating softens the experimental alloys. Especially at high strain rates of 10 and 1 s^{-1}, the corrected flow stress curves in consideration of both the effects of temperature rise and friction are even higher than the measured original ones, which demonstrates that the effect of temperature rise is more significant than that of friction. However, the influence of temperature rise will be weakened with decreasing the strain rate (Figs. 2(c)−(e)), and the flow stress curves modified according to these two correction models coincide with each other at low strain rates of 0.01 and 0.001 s^{-1} (Figs. 2(d) and (e)). It indicates that there is almost no temperature rise on account of sufficient time for the heat dissipation at low strain rate. What is more, it should be pointed out that the flow stress at high strain rates (10 and 1 s^{-1}) decreases with increasing the strain from about 0.47 to the end point. This may attribute to the systematic error resulting from the lingering performing of the counter system in the approached end of one test.

Figure 3 shows the corrected peak stress at various strain rates and temperatures. It is found that the peak stress increases with increasing the strain rate at a given temperature. Furthermore, the peak stress decreases with increasing the temperature at a given strain rate. Comparing the influence of temperature and strain rate on the flow stress in Figs. 2 and 3, it can be found that the latter is more notable.

3.2 Flow behavior and microstructure

As shown in Fig. 2, the flow stress curves exhibit typical dynamic softening during the compression process, and are evidently influenced by the strain, temperature and strain rate. With increasing the strain, the flow stress increases rapidly up to a peak stress (σ_{p}), and then decreases or keeps stable. This feature indicates flow softening such as dynamic recovery and recrystallization during the hot compression deformation [18,19]. The initial elastic deformation process is short and the stress rise is associated with work-hardening as a result of an increase of dislocation density. However, due to dynamic recovery and dynamic recrystallization, the dislocation density will not increase

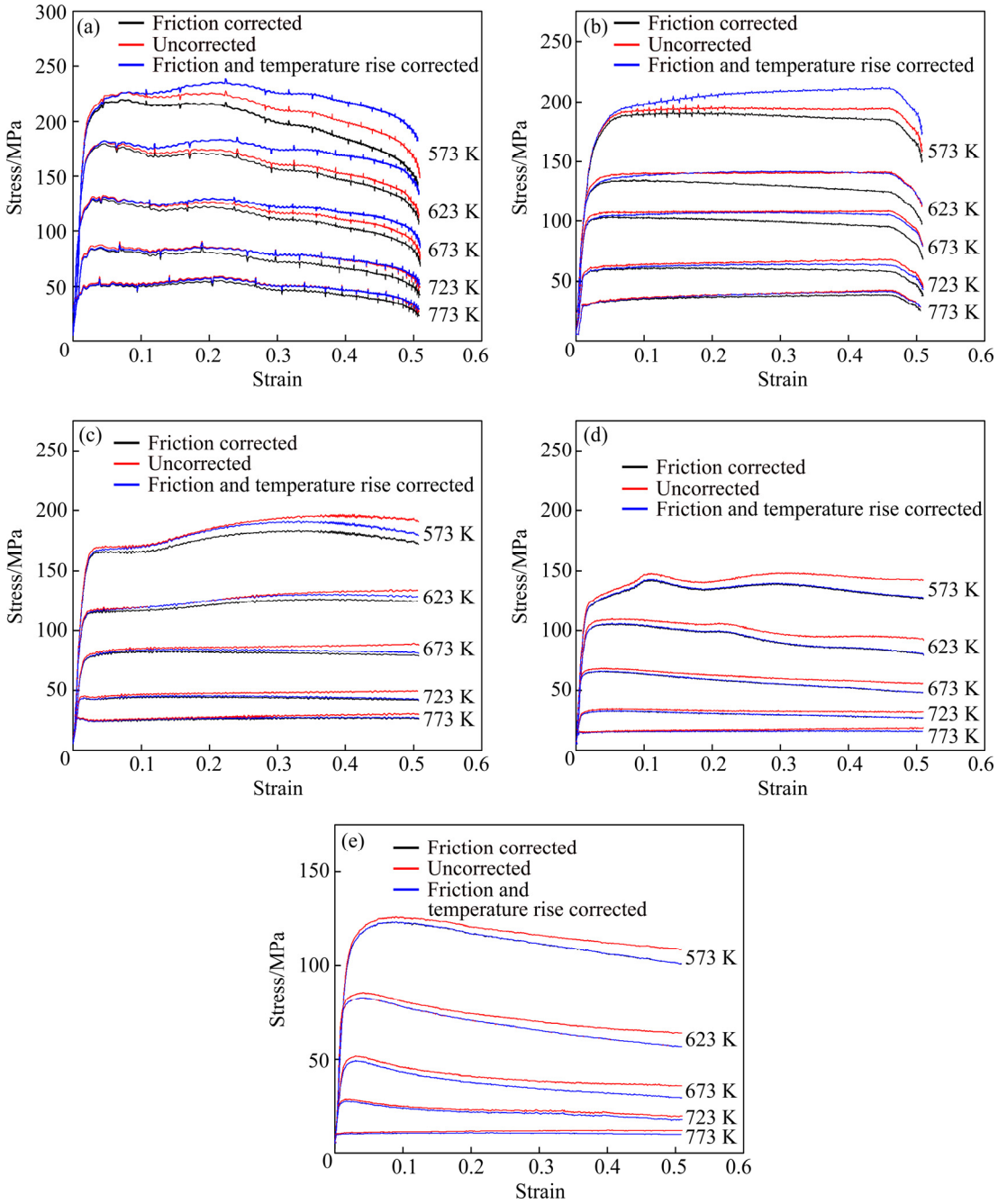

Fig. 2 Corrected and uncorrected flow stress−strain curves of 1460 Al−Li alloy compressed at strain rates of 10 s^{-1} (a), 1 s^{-1} (b), 0.1 s^{-1} (c), 0.01 s^{-1} (d) and 0.001 s^{-1} (e)

limitlessly. At high strain rates (10 and 1 s^{-1}) and all temperatures, strain rate of 0.1 s^{-1} and temperatures from 573 to 673 K, and strain rate of 0.01 s^{-1} and temperature of 573 K, there is a dynamic equilibrium between work-hardening and dynamic softening. At low strain rates (0.001 and 0.01 s^{-1}) and temperatures from 623 to 773 K, and strain rate of 0.1 s^{-1} and high temperatures of 723 and 773 K, dynamic softening possesses more notable influence on the flow stress than work-hardening, and the stress curves show a gradual decreasing tendency after the peak stress. The former is caused by dynamic recovery, which is typical of high stacking-fault-energy Al alloy [20]. The latter exhibits dynamic recrystallization due to microstructural instabilities [17], such as regular arrangement of cell structures, the growth of clear grain boundary and dynamic variation of second phases during the deformation process.

The microstructures of the deformed 1460 Al−Li alloy with a strain of 0.5 are presented in Fig. 4. The specimen deformed at 10 s^{-1} and 773 K (Fig. 4(a)) is featured by equiaxed subgrains homogeneously distributing in the whole vision, which is similar to that

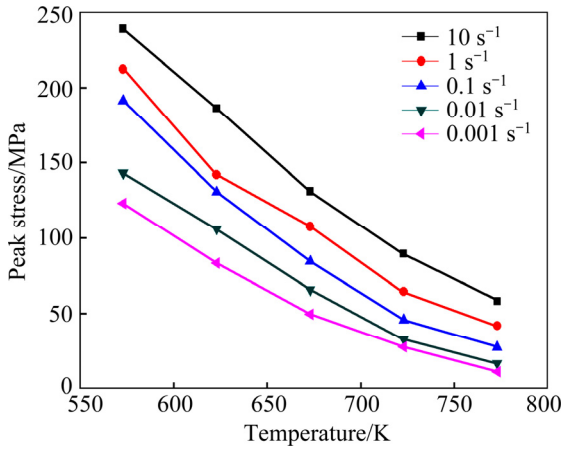

Fig. 3 Corrected peak stress as function of temperature at various strain rates

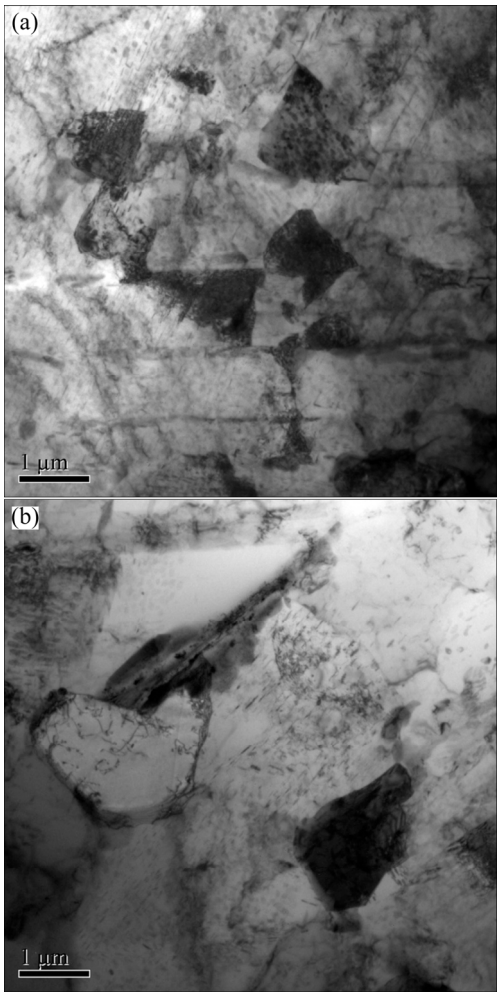

Fig. 4 TEM images of 1460 Al−Li alloy deformed at 773 K and 10 s^{-1} (a), and 573 K and 0.01 s^{-1} (b)

deformed at 0.01 s^{-1} and 573 K (Fig. 4(b)). Moreover, the TEM images show abundant dislocations tangled inside the grains, but the subgrain boundaries are vague due to their high dislocation density, exhibiting typical features of dynamic recovery.

At a given strain rate of 0.01 s^{-1}, when the deformation temperature is elevated from 573 to 773 K, the microstructure variation including second phases and dislocation density is shown in Fig. 5. As the deformation temperature is elevated to 623 K, a great amount of T_1 (Al_2CuLi) precipitates with three variants are observed (Fig. 5(a)). At 673 and 723 K, the number of T_1 precipitates decreases by dissolving into the matrix (Figs. 5(b) and (c)). Finally at 773 K, T_1 precipitates completely dissolve and disappear (Fig. 5(d)). Meanwhile, Al_3Sc particles are observed (Figs. 5(b) and (e)). It should be noted that these Al_3Sc particles form before the hot compression process and do not dissolve into the matrix during the hot compression process. In addition, the temperature rise leads to the dislocation motion and grain boundary migration more easily. Especially when the temperature is elevated to 773 K (Fig. 5(d)), there is almost no dislocation in the grain, and the grain boundary becomes straight and clear. Hence, the work-hardening at low temperatures is stronger as a result of the impediment of enough T_1 phases and dislocation-net-subgrain to dislocation motion. Thus, dynamic recrystallization and the dissolved T_1 phases result in flow softening, especially at elevated temperature higher than 673 K.

3.3 Constitutive equation of 1460 Al−Li alloy

Constitutive equations are often applied to calculating the flow stress during hot working process at set strain rates and temperatures. To model a processing stage, several constitutive functions are established by considering the non-linear distribution of strain, strain rate, temperature and their variation with time. However, a simple equation of power law, $\dot{\varepsilon} = A'\sigma^{n'}$, is not adapted to high strain rate. While a developed exponential law, $\dot{\varepsilon} = A''\exp(\beta\sigma)$ is often invalid at high temperature with strain rate below 1 s^{-1} [21,22]. Only a favorite function in Arrhenius-type is widely accepted to describe the relationship among the strain rate, flow stress (σ) and temperature. The Arrhenius hyperbolic law that gives a description between the Zener−Hollomon parameter (Z) and flow stress can be expressed as follows [23,24]:

$$A[\sinh(\alpha\sigma)]^n = \dot{\varepsilon}\exp(\frac{Q}{RT}) = Z \quad (7)$$

In the above equations, A(A', A''), α, β, n and n' are the material constants. The gas constant R is 8.314 J/(mol·K) and Q represents the hot deformation activation energy. For Al alloys, the parameter σ is generally accepted as peak stress (σ_p), even though steady rheological stress (σ_s) is also applied in Refs. [25,26]. Dynamic softening may result in a steady rheological stress (σ_s), but that is often hard to be

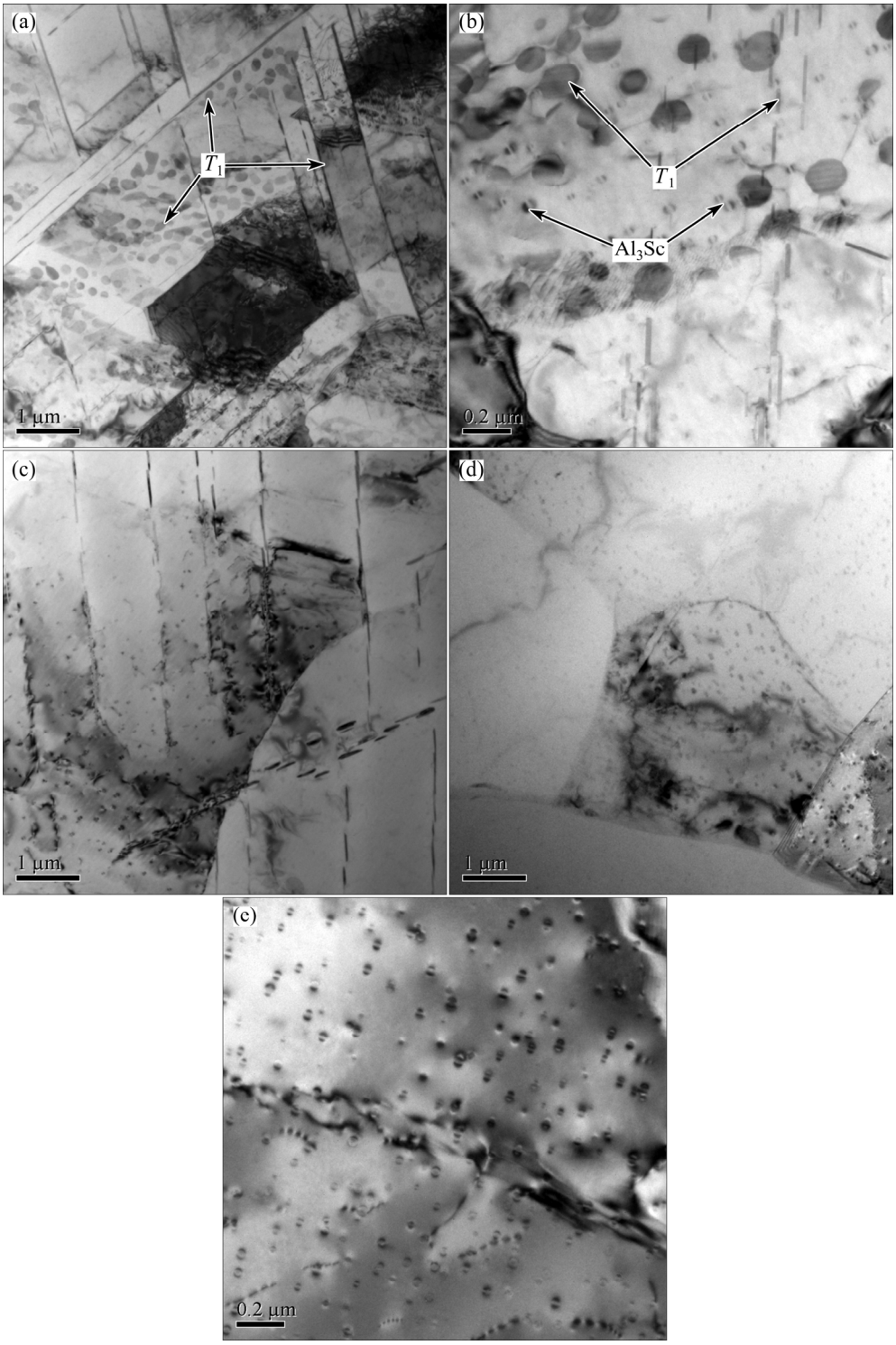

Fig. 5 TEM images of 1460 Al−Li alloy deformed at strain rate of 0.01 s^{-1} and temperatures of 623 K (a), 673 K (b), 723K (c) and 773 K (d, e)

precisely measured due to the large calculation deviation from the flow curves and morphological evolution of materials during the deformation process [27]. Therefore, the flow stresses in Eqs. (1), (4) and (7) are usually evaluated as the peak stress (σ_p) that has revealed good performance on various alloys, e.g., steel [27], magnesium alloy [28], titanium alloy [29] and nickel alloy [30]. In this study, the peak stress (σ_p) is employed, and its value is measured from the corrected flow stress curves taking account into the effect of temperature rise and friction.

The stress multiplier α varying from 0.01 to 0.08 MPa^{-1} is an important parameter for flow behavior analysis. Usually, the value of α for Al alloys is often

defined as $\alpha \approx \beta/n'$, in which β and n' are the average slopes through linear fitting of the plots of $\ln\dot{\varepsilon}$ versus σ and $\ln\dot{\varepsilon}$ versus $\ln\sigma$, respectively (Fig. 6). In this investigation, the value of α is calculated as 0.01285 MPa^{-1}.

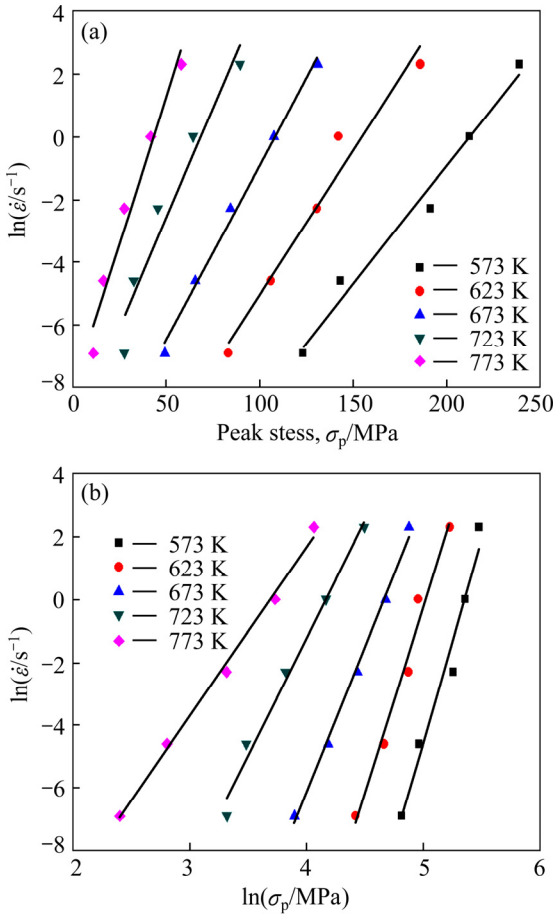

Fig. 6 Evaluation of values of β by plotting $\ln\dot{\varepsilon}$ vs σ (a) and n' by plotting $\ln\dot{\varepsilon}$ vs $\ln\sigma$ (b)

According to Eq. (7), there exist linear relationships of ln[sinh($\alpha\sigma$)] versus $\ln\dot{\varepsilon}$ and ln[sinh($\alpha\sigma$)] versus $1/T$. In addition, through the transformation of Eq. (7), the hot deformation activation energy Q can be calculated as follows:

$$Q = Rn\left\{\frac{\partial[\ln(\sinh(\alpha\sigma))]}{\partial(1/T)}\right\}_{\dot{\varepsilon}} \tag{8}$$

$$n = \left\{\frac{\partial(\ln\dot{\varepsilon})}{\partial[\ln(\sinh(\alpha\sigma))]}\right\}_{T} \tag{9}$$

Figure 7 shows the linear relevant fitting of ln[sinh($\alpha\sigma$)] versus $\ln\dot{\varepsilon}$ and ln[sinh($\alpha\sigma$)] versus $1/T$, and the R^2 value is higher than 0.96 in the temperature range of 573−773 K. The deformation activation energy (Q) of 1460 Al−Li alloy is therefore calculated as approximately 303.14 kJ/mol, which is higher than that of other reported Al−Li alloys [4−6].

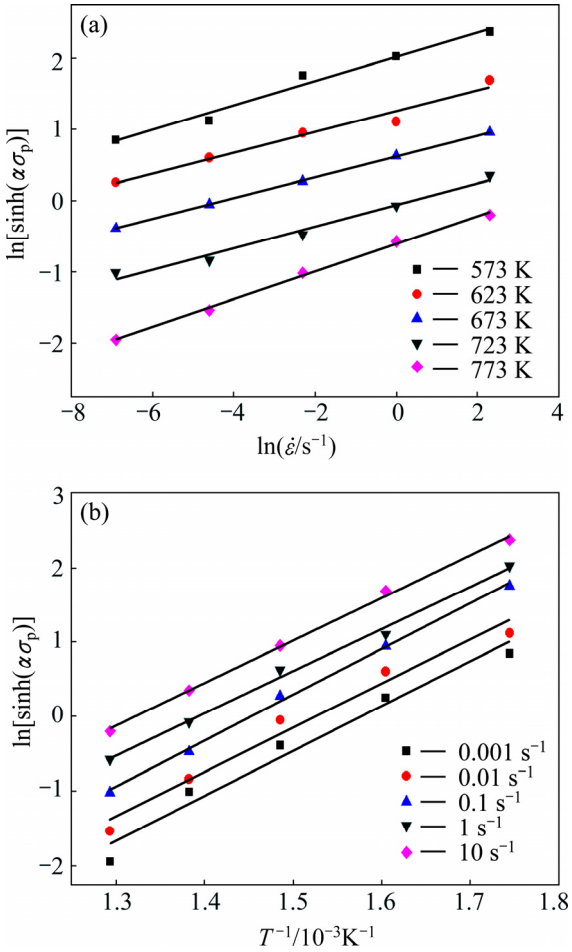

Fig. 7 Evaluation of values of n by plotting ln[sinh($\alpha\sigma$)] vs $\ln\dot{\varepsilon}$ (a) and Q by plotting ln[sinh($\alpha\sigma$)] vs $1/T$ (b)

The Zener−Hollomon parameter is generally utilized to characterize the co-effect of the control parameters of $\dot{\varepsilon}$ and T on the deformation resistance (i.e., the deformation activation energy Q). Equation (7) can be rewritten as the following equation containing parameter Z:

$$\ln Z = \ln A + n\ln[\sinh(\alpha\sigma)] \tag{10}$$

The calculated values of ln Z for 1460 Al−Li alloy at different strain rates with various temperatures are presented in Table 2. The plot of ln Z versus ln[sinh($\alpha\sigma$)] is conducted in Fig. 8, which indicates a good linear relationship with a R^2 value greater than 0.97. Hence, the values of stress exponent n and constant A can be determined as 6.17 and 1.17×10^{22}, respectively. Besides, it is evident that Z increases with increasing the strain rate, but decreases with increasing the deformation temperature, with the variation tendency similar to that of peak flow stress.

According to Eq. (7), SELLARS and MCTEGART [31] proposed a comprehensive hyperbolic sine function (Eq. (11(a))) to describe the relationships among stress, strain rate and temperature, which is expressed as

Table 2 Values of ln Z for 1460 Al−Li alloy under various deformation conditions

$\dot{\varepsilon}$ /s^{-1}	ln Z				
	573 K	623 K	673 K	723 K	773 K
0.001	58.884	53.605	49.110	45.239	41.865
0.01	61.186	55.907	51.413	47.539	44.167
0.1	63.489	58.210	53.715	49.842	46.470
1	65.791	60.512	56.018	52.145	48.772
10	65.915	60.815	56.465	52.720	49.459

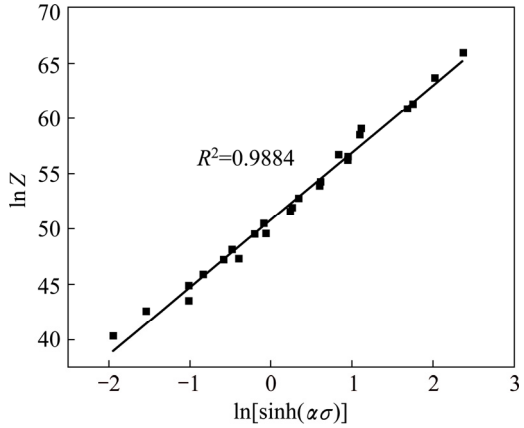

Fig. 8 Plot of ln[sinh($\alpha\sigma$)] vs ln Z under various deformation conditions

$$\dot{\varepsilon} = A[\sinh(\alpha\sigma)]^n \exp\left(-\frac{Q}{RT}\right) \quad (11(a))$$

Taking the calculated values of material constants (Table 3) into Eq. (11(a)), a constitutive equation of 1460 Al−Li alloy is established as follows:

$$\dot{\varepsilon} = 1.17\times10^{22}[\sinh(0.01285\sigma)]^{6.17}\exp\left(-\frac{303.14}{RT}\right) \quad (11(b))$$

Table 3 Values of material constants for 1460 Al−Li alloy

α/MPa^{-1}	n	A	Q/(kJ·mol^{-1})
0.01285	6.17	1.17×10^{22}	303.14

3.4 Validity evaluation of constitutive equation

Since the constitutive equation is applied to predicting and guiding the actual processing, the validity of the established constitutive equation (Eq. (11(b))) for 1460 Al−Li alloy is therefore evaluated through comparing the corrected experimental peak stress and predicted data (Table 4 and Fig. 9). It can be seen that the predicted peak stress values can well track the corrected experimental data. Most of the relative error range is restricted within 8%. Only at strain rate of 0.001 s^{-1} and temperatures of 673 and 723 K, the relative error is up to 21%. Meanwhile, at the lowest strain rate of 0.001 s^{-1}, the deviation between the peak stress and the corrected experimental one is higher, which probably results from a higher dynamic softening (dynamic recovery and dynamic recrystallization). Further work for the particular analysis of these two processes still needs to be done in this direction to draw a firm conclusion.

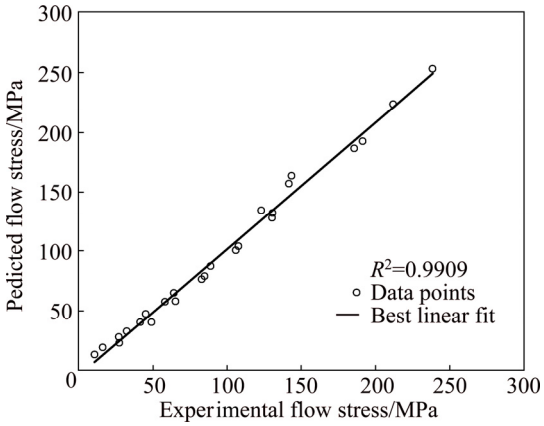

Fig. 9 Correlation between corrected experimental and predicted flow stresses from developed constitutive equation

The validity of the constitutive equation is also evaluated by a standard statistical parameter called average absolute relative error (AARE), which is expressed as follows [32]:

$$\delta_{\mathrm{AARE}} = \frac{1}{N}\sum_{i=1}^{N}\left|\frac{\sigma_{i,\mathrm{exp.}}-\sigma_{i,\mathrm{cal.}}}{\sigma_{i,\mathrm{cal.}}}\right|\times100\% \quad (12)$$

where N is the number of data employed in the investigation. $\sigma_{i,\mathrm{exp.}}$ and $\sigma_{i,\mathrm{cal.}}$ are the values of corrected experimental stress and calculated flow stress,

Table 4 Calculated and corrected experimental flow stresses of 1460 Al−Li alloy at various temperature with different strain rates

$\dot{\varepsilon}$ /s^{-1}	573 K			623 K			673 K			723 K			773 K		
	Cal./ MPa	Exp./ MPa	Error/ %	Cal./ MPa	Exp./ MPa	Error/ %	Cal./ MPa	Exp./ MPa	Error/ %	Cal./ MPa	Exp./ MPa	Error/ %	Cal./ MPa	Exp./ MPa	Error/ %
10	253.1	238.8	5.65	186.4	186.0	0.20	131.2	131.0	0.12	87.7	89.5	−1.97	56.8	58.1	−2.37
1	222.9	212.1	4.86	156.8	142.1	9.38	103.7	107.6	−3.74	65.0	64.4	0.89	40.1	41.8	−4.21
0.1	192.8	191.3	0.79	128.0	130.6	−2.06	78.8	84.5	−7.19	46.5	45.7	0.84	27.8	27.6	1.81
0.01	163.1	143.2	12.23	100.8	106.0	−5.22	57.6	65.7	−14.12	32.5	32.7	−0.75	19.0	16.6	12.89
0.001	134.1	123.2	8.18	76.2	83.2	−9.14	40.7	49.3	−21.09	22.3	27.7	−23.99	13.0	11.1	14.64

respectively. Although there are some scattering data points at strain rate of 0.001 s^{-1} and 673 and 723 K, there exists a good linear relationship between the corrected experimental and predicted ones. The linear correlation coefficient and AARE are calculated to be 0.9909 and 6.72%, respectively, which reflects the effective prediction capabilities of the proposed constitutive equation.

4 Conclusions

1) The corrected flow stress−strain curves of 1460 Al−Li alloy during hot compression process at elevated temperatures from 573 to 773 K with strain rates ranging from 10 to 10^{-3} s^{-1} are reasonable to describe the hot behavior of 1460 Al−Li alloy. Compared with the original ones, the flow stress curves ascend after the friction correction, and the difference increases with increasing the strain rate. While after the temperature rise correction and the friction correction, there exist no changes in flow stress curves at low strain rates (0.01 and 0.001 s^{-1}) and there is a greater descending trend at high strain rates.

2) At temperatures higher than 673 K and lower strain rates (0.001, 0.01 and 0.1 s^{-1}), dynamic recrystallization and the dissolution of T_1 phases are recognized as the reasons of flow softening in 1460 Al−Li alloy. Furthermore, dynamic recovery predominantly occurs at low temperatures and high strain rates.

3) The constitutive material constants, α, n, A and Q, for 1460 Al−Li alloy are determined from the corrected experimental data under all deformation conditions. On the basis of these parameters and the Arrhenius-type constitutive model, the constitutive equation of 1460 Al−Li alloy during hot compression is established as follows:

$$\dot{\varepsilon} = 1.17\times10^{22}[\sinh(0.01285\sigma)]^{6.17}\exp\left(-\frac{303.14}{RT}\right).$$

The established constitutive equation has good prediction capabilities throughout the entire temperature and strain rate range except for strain rate of 0.001 s^{-1} with temperatures of 673 and 723 K.

References

[1] RIOJA J R, LIU J. The evolution of Al−Li base products for aerospace and space applications [J]. Metallurgical and Materials Transactions A, 2012, 43(9): 3325−3337.

[2] WILLIAMS J C, STARKE E A. Progress in structural materials for aerospace systems [J]. Acta Materialia, 2003, 51(19): 5775−5799.

[3] LI Jin-feng, CHEN Wen-jing, ZHAO Xu-shan, REN Wen-da, ZHENG Zi-qiao. Corrosion behavior of 2195 and 1420 A1−Li alloys in neutral 3.5% NaCl solution under tensile stress [J]. Transactions of Nonferrous Metals Society of China, 2006, 16(5): 1171−1177.

[4] OU Ling, NIE Yu-feng, ZHENG Zi-qiao. Strain compensation of the constitutive equation for high temperature flow stress of a Al−Cu−Li alloy [J]. Journal of Materials Engineering and Performance, 2014, 23(1): 25−30.

[5] AVRAMOVIC-CINGARA G, MCQUEEN H J, PEROVIC D D. Comparison of torsion and compression constitutive analyses for elevated temperature deformation of Al−Li−Cu−Mn alloy [J]. Materials Science and Technology, 2003, 19(1): 11−19.

[6] AVRAMOVIC-CINGARA G, PEROVIC D, MCQUEEN H J. Hot deformation mechanisms of a solution-treated Al−Li−Cu−Mg−Zr alloy [J]. Metallurgical and Materials Transactions A, 1996, 27(11): 3478−3490.

[7] LAASRAOUI A, JONAS J. Prediction of steel flow stresses at high temperatures and strain rates [J]. Metallurgical and Materials Transactions A, 1991, 22(7): 1545−1558.

[8] LIN Yong-cheng, LIU Ge. A new mathematical model for predicting flow stress of typical high-strength alloy steel at elevated high temperature [J]. Computational Materials Science, 2010, 48(1): 54−58.

[9] LANGKRUIS J, KOOL W H, ZWAAG S. Assessment of constitutive equations in modeling the hot deformability of some overaged Al−Mg−Si alloys with varying solute contents [J]. Materials Science and Engineering A, 1999, 266(1−2): 135−145.

[10] EBRAHIMI R, NAJAFIZADEH A. A new method for evaluation of friction in bulk metal forming [J]. Journal of Materials Processing Technology, 2004, 152(2): 136−143.

[11] FREDERIKSEN N, WANHEIM T. Development of friction test for lubrication in model-material experiments [J]. Journal of Mechanical Working Technology, 1985, 12(2): 261−268.

[12] BAY N. Friction stress and normal stress in bulk metal forming processes [J]. Journal of Mechanical Working Technology, 1987, 14(2): 203−223.

[13] VENUGOPAL S, SRINIVASAN G, VENKADESOAN S, SEETHARAMAN V. A note on the determination of the friction factor by means of the reduction-capacity test [J]. Journal of Mechanical Working Technology, 1989, 19(2): 261−266.

[14] GOETZ R L, SEMIATIN S L. The adiabatic correction factor for deformation heating during the uniaxial compression test [J]. Journal of Materials Engineering and Performance, 2001, 10(6): 710−717.

[15] LI Hui-zhong, WEI Xiao-yan, OUYANG Jie, JIANG Jun, LI Yi. Hot deformation behavior of extruded AZ80 magnesium alloy [J]. Transactions of Nonferrous Metals Society of China, 2013, 23(11): 3180−3185.

[16] OH S I, SEMIATIN S L, JONAS J J. An analysis of the isothermal hot compression test [J]. Metallurgical Transactions A, 1992, 23(3): 963−975.

[17] GEORGE E D, HOWARD A K, SEMIATIN S L. Handbook of workability and process design [M]. Chio, USA: ASM International, 2003: 35−44.

[18] MCQUEEN H J, IMBERT C A C. Dynamic recrystallization: Plasticity enhancing structural development [J]. Journal of Alloys and Compounds, 2004, 378(1−2): 35−43.

[19] FANG Y L, LIU Z Y, SONG H M, JIANG L Z. Hot deformation behavior of a new austenite–ferrite duplex stainless steel containing high content of nitrogen [J]. Materials Science and Engineering A, 2009, 526(1−2): 128−133.

[20] MCQUEEN H J, HOCKETT J E. Microstructures of aluminum compressed at various rates and temperatures [J]. Metallurgical Transactions, 1970, 1(11): 2997−3004.

[21] RYAN N D, MCQUEEN H J. Mean pass flow stresses and interpass softening in multistage processing of carbon-, HLSA-, tool- and γ-stainless steels [J]. Journal of Mechanical Working Technology, 1986, 12(3): 323−349.

[22] RYAN N D, MCQUEEN H J. Stainless steels [M]. London: ASTM International, 1987: 498−507.
[23] ZENER C, HOLLOMON J H. Effect of strain rate upon plastic flow of stee [J]. Journal of Applied Physics, 1944, 15(1): 22−32.
[24] MCQUEEN H J, YUE S, RYAN N D, FRY E. Hot working characteristics of steels in austenitic state [J]. Journal of Materials Processing Technology, 1995, 53(1−2): 293−310.
[25] LIU Wen-yi, ZHAO Huan, LI Dan, ZHANG Zi-qing, HUANG Guan-jie, LIU Qing. Hot deformation behavior of AA7085 aluminum alloy during isothermal compression at elevated temperature [J]. Materials Science and Engineering A, 2014, 596: 176−182.
[26] PRASAD Y V R K, SASIDHARA S, SIKKA V K. Characterization of mechanisms of hot deformation of as-cast nickel aluminide alloy [J]. Intermetallics, 2002, 8(9−11): 987−995.
[27] MCQUEEN H J, RYAN N D. Constitutive analysis in hot working [J]. Materials Science and Engineering A, 2002, 322(1−2): 43−63.
[28] GALL S, HUPPMANN M, MAYER H M, REIMERS W. Hot working behavior of AZ31 and ME21 magnesium alloys [J]. Journal of Materials Science, 2013, 48: 473−480.
[29] FAN J K, KOU H C, LAI M J, TANG B, CHANG H, LI J S. Hot deformation mechanism and microstructure evolution of a new near β titanium alloy [J]. Materials Science and Engineering A, 2013, 584: 121−132.
[30] WU H Y, ZHU F J, WANG W R, WANG C C, CHIU C H. Hot deformation characteristics and strain-dependent constitutive analysis of Inconel 600 superalloy [J]. Journal of Materials Science, 2012, 47: 3971−3981.
[31] SELLARS C M, MCTEGART W J. On the mechanism of hot deformation [J]. Acta Metallurgica, 1966, 14(9): 1136−1138.
[32] SRINIVASULU S, JAIN A. Comparative analysis of training methods for artificial neural network rainfall-runoff models [J]. Applied Soft Computing, 2006, 6(3): 295−306.

1460 铝锂合金热变形行为及其组织演变

向 胜[1]，刘丹阳[1]，朱瑞华[1]，李劲风[1]，陈永来[2]，张绪虎[2]

1. 中南大学 材料科学与工程学院，长沙 410083；
2. 航天材料及工艺研究所，北京 100076

摘 要：通过等温热压缩实验，综合研究 1460 铝锂合金在不同应变速率(10^{-3}~10 s^{-1})和不同温度(573~773 K)下的热变形行为及其组织演变规律。通过考虑压板和样品界面的摩擦力和形变热导致的温度变化，对流变应力曲线进行校正。结合变形行为中的应变、应变速率和温度的影响，可以通过正弦关系中的 Z 参数来描述其变形行为，并根据动态回复、动态再结晶、T_1 相的溶解对峰值流变应力的影响，建立 1460 铝锂合金的本构方程。在所有应变速率和温度范围内，本构方程有效性验证表明，改进后的本构方程是可行有效的，其线性相关系数和相对误差分别为 0.9909 和 6.72%。

关键词：1460 铝锂合金；摩擦修正；温升修正；本构方程；热变形行为

(Edited by Mu-lan QIN)